EMBRY-RIDDLE
Aeronautical University
SCHOLARLY COMMONS

Publications

3-1990

A Simulation and Diagnostic Study of Water Vapor Image Dry Bands

Bradley M. Muller
Florida State University, mullerb@erau.edu

Henry E. Fuelberg
Florida State University

Follow this and additional works at: https://commons.erau.edu/publication

 Part of the Atmospheric Sciences Commons, and the Meteorology Commons

Scholarly Commons Citation

Muller, B. M., & Fuelberg, H. E. (1990). A Simulation and Diagnostic Study of Water Vapor Image Dry Bands. *Monthly Weather Review, 118*(3). https://doi.org/10.1175/1520-0493(1990)118<0705:ASADSO>2.0.CO;2

© Copyright 1990 American Meteorological Society (AMS). Permission to use figures, tables, and brief excerpts from this work in scientific and educational works is hereby granted provided that the source is acknowledged. Any use of material in this work that is determined to be "fair use" under Section 107 of the U.S. Copyright Act September 2010 Page 2 or that satisfies the conditions specified in Section 108 of the U.S. Copyright Act (17 USC §108, as revised by P.L. 94-553) does not require the AMS's permission. Republication, systematic reproduction, posting in electronic form, such as on a web site or in a searchable database, or other uses of this material, except as exempted by the above statement, requires written permission or a license from the AMS. Additional details are provided in the AMS Copyright Policy, available on the AMS Web site located at (https://www.ametsoc.org/) or from the AMS at 617-227-2425 or copyrights@ametsoc.org.
This Article is brought to you for free and open access by Scholarly Commons. It has been accepted for inclusion in Publications by an authorized administrator of Scholarly Commons. For more information, please contact commons@erau.edu.

A Simulation and Diagnostic Study of Water Vapor Image Dry Bands

BRADLEY M. MULLER AND HENRY E. FUELBERG

Department of Meteorology, Florida State University, Tallahassee, Florida

(Manuscript received 28 March 1989, in final form 19 September 1989)

ABSTRACT

A Limited Area Mesoscale Prediction System (LAMPS) model simulation and special 3-hour radiosonde dataset are used to investigate warm (dry) bands in 6.7 μm water vapor satellite imagery on 6–7 March 1982. The purpose is to reveal processes resulting in the formation and evolution of the dry features that appear as curving dark streaks in the imagery. Model soundings are input to a radiative transfer algorithm to generate synthetic 6.7 μm equivalent blackbody temperatures (T_B) which are compared with those from the Visible Infrared Spin Scan Radiometer Atmospheric Sounder aboard the Geostationary Operational Environmental Satellite. Simulated and radiosonde-derived vertical velocity and humidity also are compared with the images. Finally, trajectories are calculated from both radiosonde data and LAMPS output.

The model reproduces major characteristics of the observed T_B field. A "development" dry image feature occurs in conjunction with an upper level shortwave trough, and an "advective" feature is associated with a polar jet streak. Both model and observed T_B features are associated with vorticity maxima. The development feature forms as moisture gradients are enhanced by differential subsidence early in the study period. Horizontal wind shear then narrows the incipient dry area into its streak-like shape. Trajectories reveal that air parcels ending in the development streak move with it, in northwesterly, subsiding flow throughout the study period. Near the leading edge of the streak, ahead of the short-wave trough, flow is southwesterly and ascending. Air parcels in the advective image feature sink in the wake of the vorticity maximum, move through it in the jet flow, and finally ascend ahead of it. Thus, warm T_B regions do not equate with instantaneous subsidence patterns, but reflect a long history of parcel motions which can include ascent as well.

1. Introduction

Many recent satellites have included radiometric sensors with a 6.7 μm channel, known as a "water vapor" channel because measured radiances are associated with middle to upper tropospheric moisture content. One example is the Visible Infrared Spin Scan Radiometer (VISSR) Atmospheric Sounder (VAS) aboard the GOES (Geostationary Operational Environmental Satellite) platform. Pronounced bands of warm equivalent blackbody temperatures (T_B) often are detected in water vapor imagery. Such bands denote dry air and are a common signature that has been associated with surface cyclogenesis (Uccellini et al. 1985; Reed and Albright 1986; Young et al. 1987), the initiation of convection and severe weather (Petersen et al. 1984; Rodgers et al. 1985), the presence of upper level jet streaks, tropopause folding, and tropical cyclones (Velden 1987).

A promising research area into satellite imagery incorporates numerical modeling techniques. Specifically, models can provide important "data" for diagnostic meteorological studies (Keyser and Uccellini 1987), yielding resolution unobtainable from the operational radiosonde network. For example, Rodgers et al. (1976) used a 10-level diagnostic model to associate tropospheric kinematics quantitatively with observed 6.7 μm water vapor features. Their case study demonstrated that increasing T_B's were associated with horizontal advection of previously subsided air that was augmented by ongoing descent. More recently, Durran and Weber (1988) simulated cirrus cloud shields associated with midlatitude jet streams, and Young et al. (1987) used the British Meteorological Office operational fine mesh model to relate the origin and structure of a "dry intrusion" seen in water vapor images to rapid cyclogenesis.

Numerical models also have been used to forecast satellite imagery. The Petersen and Homan (1989) isentropic advective scheme produced forecasts of VAS water vapor imagery that simulated some aspects of differential moisture advection leading to convection, but was unable to fully capture an observed increase in T_B attributed to subsidence.

The current study uses model temperature and humidity soundings as input to a radiative transfer algorithm that simulates satellite detected T_B's in the 6.7 μm channel. The purpose is to employ high resolution model output as a tool for investigating atmospheric processes associated with warm (dry) image bands on

Corresponding author address: Dr. Henry E. Fuelberg, Department of Meteorology, The Florida State University, Tallahassee, FL 32306-3034.

© 1990 American Meteorological Society

6–7 March 1982. This research differs in two important respects from previous investigations using models with satellite imagery. First, specific simulated image features can be related directly to model kinematic processes because the synthetic images are dynamically consistent with the model output. None of the above-mentioned studies used model soundings to simulate T_B. Second, 3-hour radiosonde releases during the study period provide high resolution "ground truth" of model atmospheric processes.

The paper includes six major sections. Section 2 discusses radiative transfer and its relationship to water vapor imagery. Section 3 describes the models and data procedures, while section 4 contains a synoptic summary of the period. A verification of simulated versus observed T_B images is given in section 5, followed by an analysis of model output and observed radiosonde-derived data to determine causes for specific image features. Finally, conclusions about those causes are summarized in section 6.

2. Radiative transfer considerations

Water vapor imagery at 6.7 μm represents conditions over a broad layer of the atmosphere, primarily sensing the top few millimeters of precipitable water (Chesters et al. 1982). Poc et al. (1980), Fischer et al. (1981) and Ramond et al. (1981) have addressed aspects of image interpretation. Weldon and Holmes (1984) noted that factors determining the intensity of upwelling 6.7 μm radiation include the total amount of water vapor, its vertical distribution, associated temperature patterns, and the satellite zenith angle. As quantified in the radiative transfer equation (e.g., Liou 1980), the measured radiance or T_B represents contributions from a "surface" term incorporating the emitting temperature of either the earth or a cloud surface, and the vertically integrated effects of atmospheric moisture and temperature.

For cloud-free skies, the atmospheric term generally dominates the surface term due to absorption and reradiation of surface energy by water vapor aloft. Less radiation reaches a satellite from higher and cooler layers than is emitted at the surface. Thus, Weldon and Holmes noted that for typical temperature profiles having no inversions, the usual effect of moisture is to decrease the T_B. In the case of upper level cloud decks, the (cloud) surface term often dominates, with the clouds appearing as relatively cold image signatures due to their cold emission temperatures. Low clouds usually have very little effect on 6.7 μm imagery due to absorption and reradiation by the water vapor above.

Atmospheric water vapor usually is not well mixed in the vertical, complicating image interpretation. The vertical derivative of transmittance, or weighting function, describes the contribution of radiance at a particular level to the total radiance reaching the satellite. Weldon and Holmes showed that moist layers existing at both upper and lower levels produce a weighting function with two peaks. They also noted that a single moist layer at different levels can result in similar T_B's. For example, a humid region near 300 mb can yield the same T_B as a moist layer near 700 mb. For a standard atmosphere, however, the weighting function of the GOES VAS 6.7 μm channel peaks at approximately 400 mb, with the greatest contribution emanating from between 800 and 200 mb.

One of the least ambiguous interpretation scenarios occurs when the middle and upper troposphere are very dry. Petersen et al. (1984) pointed out that the resulting warm T_B's will contrast sharply with cold values from surrounding midlevel moist areas. Since cold T_B's are represented by light image shades while warmer T_B's are depicted by darker shades, the moist areas appear as relatively light tones while the drier regions appear darker. Despite some uncertainty about the vertical moisture distribution in the lighter areas, the dark areas always reflect a comparatively dry middle and upper troposphere. The current study concentrates on such dry (warm) image features on 6–7 March 1982.

3. Methodology

Data for the study period included observed VAS 6.7 μm T_B's, radiosonde observations (RAOBS) from the Atmospheric Variability Experiment/VAS Ground Truth Experiment (AVE/VAS), and model output from the Limited Area Mesoscale Prediction System (LAMPS, Perkey 1976). RAOBS were available at 1100, 1445, 1745, 2045, 2345 and 0245 UTC 6–7 March from a special mesoscale network (see Jedlovec 1985) and National Weather Service sites.

LAMPS is a hydrostatic, primitive equation, mesoscale model. The version employed here had 15 sigma-height levels, a horizontal grid spacing of approximately 70 km, fixed sponge boundaries, and a domain within 23.625°–43.625°N and 80°–107°W. The model initial state was derived from objectively analyzed radiosonde data at 1200 UTC 6 March, and the simulation ended at 0400 UTC 7 March. The LAMPS output used here was from Kalb's (1987) convective parameterization experiment.

LAMPS-derived vertical profiles of temperature and humidity were used to prepare simulated imagery at 3-hour intervals from 1200 UTC 6 March through 0300 UTC 7 March, corresponding to observed imagery at 1100, 1430, 1730, 2030, 2330 and 0230 UTC. Specifically, a modified form of the Weinreb and Hill (1980) radiative transfer code used LAMPS soundings to compute monochromatic radiances for 6.7 μm. Transmittances were obtained using the procedure of Weinreb and Neuendorffer (1973), with continuum and trace gas contributions ignored, and no provision made for model cloud areas. Effects of varying zenith angles on radiances were included. Once LAMPS-derived radiance fields were generated, a two-dimensional

smoothing operator (Shuman 1957) suppressed noise that appeared at later times of the run. The T_B's were prepared from the smoothed radiances using the monochromatic Planck function.

As noted earlier, water vapor radiances are strongly affected by middle and upper tropospheric clouds and do not represent only the atmosphere's vapor content. Thus, a comparison of observed versus simulated T_B's must consider locations of both observed and modeled cloudiness. Clouds in the observed VAS images were estimated using a split window technique (Smith 1983) in which skin temperatures calculated from T_B's of the 11 and 12 μm channels were compared with observed surface temperatures. Locations of model clouds were based on nonzero cloud water content above 750 mb.

LAMPS output was interpolated to constant pressure levels, and several diagnostic parameters then were calculated. Trajectories were estimated kinematically from the three-dimensional model wind fields following the procedure outlined by Heckley and Hoskins (1982), an extension to three dimensions of Petterssen's (1956) iterative technique.

Comparison between observed and modeled T_B's was facilitated by objectively analyzing (Barnes 1973) observed VAS images onto the LAMPS grid. Since the observed and simulated "images" enclosed somewhat different regions, a subgrid representing the common area was identified.

Vertical motions were calculated from the RAOB data. The procedure included objective analysis of wind components at 50 mb intervals onto a grid partially coincident with the LAMPS grid. The spacing of 140 km was twice that of the model version. Vertical motion estimates then were calculated from the wind fields using the kinematic method and O'Brien's (1969) second order adjustment technique. Values were assumed to be zero at the surface and 100 mb. Trajectories also were calculated from these three-dimensional wind fields, again using the Heckley and Hoskins (1982) procedure.

4. Synoptic summary

Meteorological conditions during the period are indicated in Fig. 1, and additional weather summaries are presented by Jedlovec (1985) and Fuelberg and Meyer (1986). The dominant 500 mb feature at 1200 UTC 6 March (the model initial state) was an upper level short-wave trough from Kansas to New Mexico that was advancing southeastward through the major trough. Strong temperature gradients and wind shears were associated with this system. Cold, dry air accom-

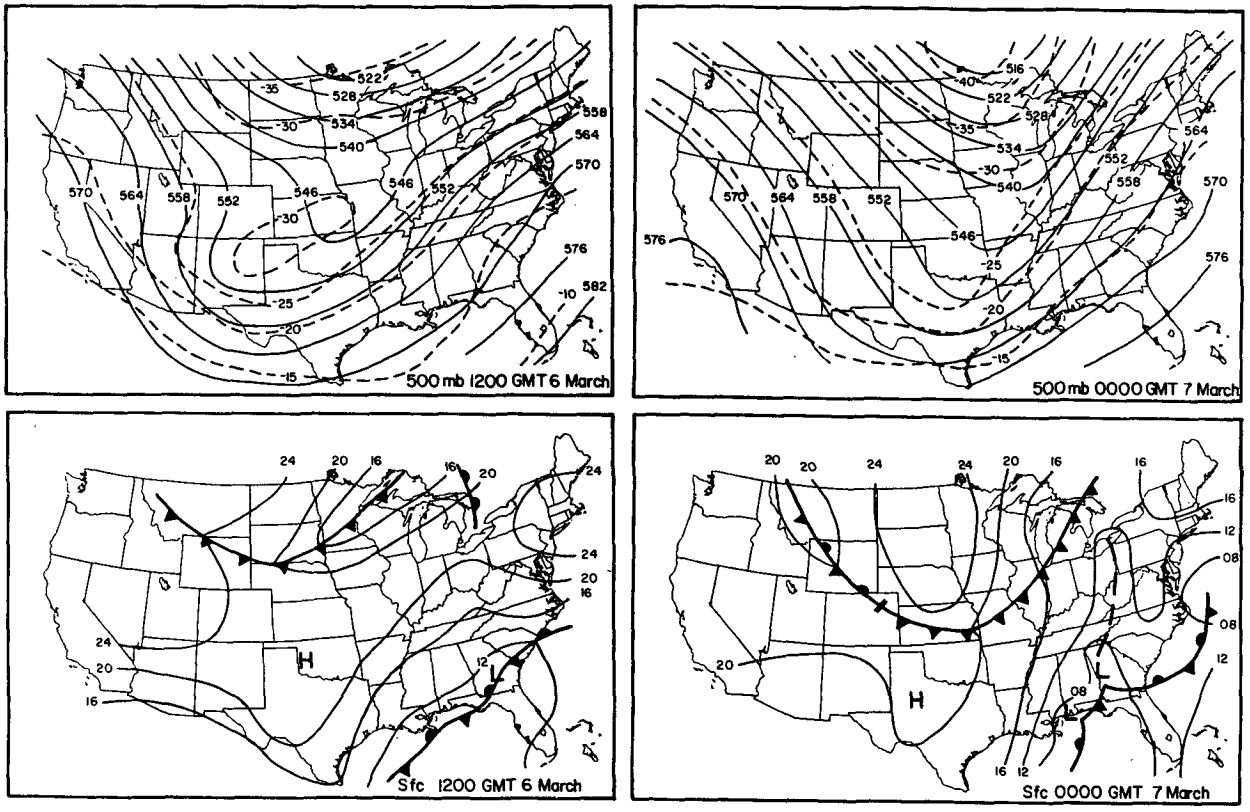

FIG. 1. Surface and 500 mb analyses for 1200 UTC 6 March (corresponding to the LAMPS initialization) and 0000 UTC 7 March 1982. Solid lines at 500 mb are height contours in decameters while dashed lines are isotherms in °C. Isobars are at 4 mb intervals.

panied the trough, with 500 mb temperatures less than −30°C and dewpoint depressions from 10° to over 30°C. At the surface, a weak cold front associated with cloudiness and light snow was advancing southward through the Northern Plains states toward the study area, while a quasi-stationary front stretched over the Gulf of Mexico. An area of rain and clouds covered East Texas, Louisiana and Mississippi, while light snow was falling over Arkansas, southern Missouri and southern Illinois.

Wind patterns at 200 and 300 mb (not shown) included complex polar and subtropical jet streams. A polar jet maximum was located over the border of Arizona/New Mexico/Mexico, propagating eastward around the base of the trough. The entrance region of a second polar jet streak was northeast of the study area, over southern Illinois. The subtropical jet stream was located along the Gulf Coast.

Near the end of the study period, at 0000 UTC 7 March (Fig. 1), the 500 mb trough stretched from eastern Texas through southeast Missouri. The minimum temperature within the 500 mb cold pocket over northeastern Texas had warmed to −29°C while dewpoints over Arkansas, Oklahoma and most of Texas had decreased further from their already low values. Much of the precipitation and cloudiness over the Gulf Coast had shifted eastward, accompanying a surface low that had developed along the quasi-stationary front. Some strong convective cells were associated with the system. The cold front over the northern plains had advanced to southern Kansas, with clouds and light snow in Iowa and upslope snow showers along the Colorado/Nebraska/Wyoming border. Despite evidence of an upper level frontal zone, there was no sign of strong surface cyclogenesis. The jet streak over the Southwest (not shown) had propagated eastward and now was over northern Mexico and extreme southern Texas, while the streak over the Ohio Valley remained nearly stationary. The subtropical jet continued along the Gulf Coast.

5. Results

a. Comparison of image features

Observed VAS 6.7 μm water vapor images (Fig. 2) reveal a pronounced warm (dark) band curving from southern Arizona through Texas and Missouri. The following discussion uses T_B analyses derived from these images (Fig. 3, top) and T_B's from the LAMPS output (Fig. 3, bottom). In each case cloud cover is denoted by scallops.

At 1100 UTC, the observed image contains relatively warm T_B values (Fig. 3) greater than 242 K over western Texas, Oklahoma, and Kansas. Moore and Fuelberg (1988) tracked the warm area over western Texas upstream to Washington on 5 March, while the warm regions over Oklahoma and Kansas developed in situ. Following Moore and Fuelberg, they are termed the "advective" and "development" features, respectively. The development feature actually is composed of dual warm bands, best seen in the 1430 and 1730 UTC images (Fig. 2). Cloudiness dominating the southeastern portion of the region produces cold T_B's.

By 1730 UTC (Fig. 3), the observed warm feature over western Texas has propagated eastward, intensified to over 246 K, and begun to merge with the T_B maximum over southeastern Oklahoma. The second component of the development feature, the warm streak initially over Kansas, has moved southeastward to central Oklahoma and strengthened to 244 K. Cloud-induced cold T_B's in the Southeast have pushed eastward. Observed values at 2030 UTC display continued merging of the warm features and expansion of the 244 and 246 K contours. By 2330 UTC, maxima have increased to 248 K as the developing portion has joined with the warm region propagating from the southwest. This advecting portion now encompasses most of Texas, while the development section, with its northern end apparently anchored over Missouri and Illinois, is rotating counterclockwise, in phase with the eastward movement of the advective feature. Finally, by 0230 UTC, maximum T_B's have increased to 250 K, with warm values now extending into Louisiana. The axis of maximum T_B stretches across southern Texas, then curves northeastward through Arkansas, Missouri, and Illinois.

LAMPS-derived T_B patterns (Fig. 3, bottom) capture many features seen in the observed versions (Fig. 3, top). Some differences are to be expected, however, arising from factors such as disparities between model and observed soundings, including their horizontal and vertical resolutions, time discrepancies between the two types of imagery, smoothing algorithms applied to both data types, and inherent limitations of the radiative transfer code, including failure to treat clouds, hydrometeors, and trace gases.

Figure 3 shows that T_B's in cloud free regions are very similar, with differences between the two types generally less than 4 K, or about 10 to 15 percent of the normal 30 K range of clear-sky 6.7 μm values. Since cloud surfaces were not treated in the radiative transfer code, simulated T_B's in cloudy areas are much too warm. Image differences early in the study period are due mostly to model spinup. For example, observed clouds at 1100 UTC cover approximately two-thirds of the domain, whereas the model has produced only a small cloudy area at 1200 UTC. In fact, the model does not yield realistic cloud coverage until 1800 UTC. This delay is probably attributable to the unsaturated and nearly nondivergent initial state (Kalb 1987). The initial analysis at 1100 UTC contains a spurious dry area in the middle and upper levels over southern Louisiana that results in excessively warm simulated T_B's. Since the anomalous region is located in the south-

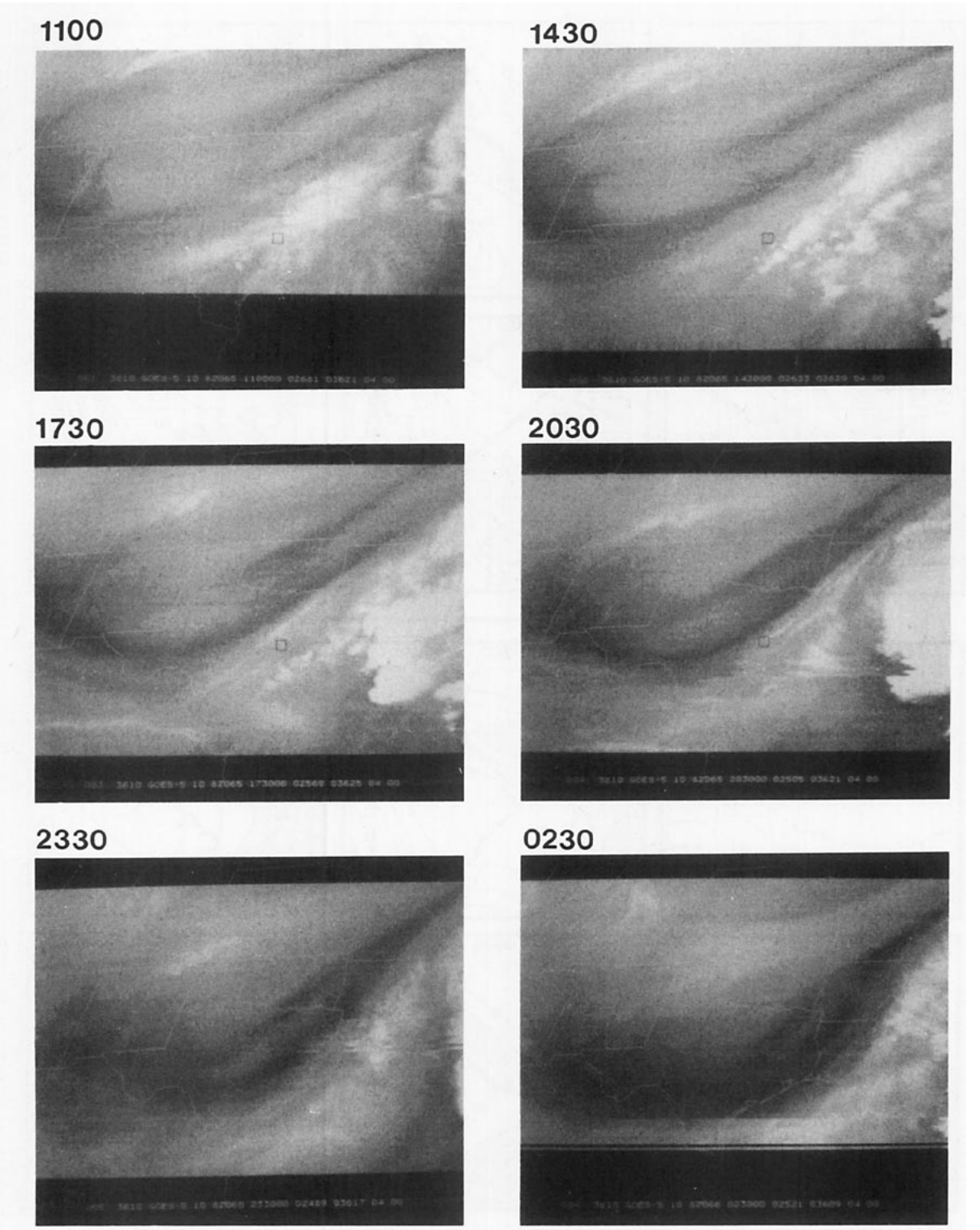

FIG. 2. Observed GOES/VAS 6.7 μm water vapor imagery on 6–7 March 1982. Times are in UTC.

eastern sector of the study area and quickly moves eastward, it is not important to the goals of this study.

An important measure of a model's success is its ability to simulate the time evolution of observed features, and LAMPS T_B forecasts (Fig. 3) generally are successful in this regard. LAMPS correctly locates the

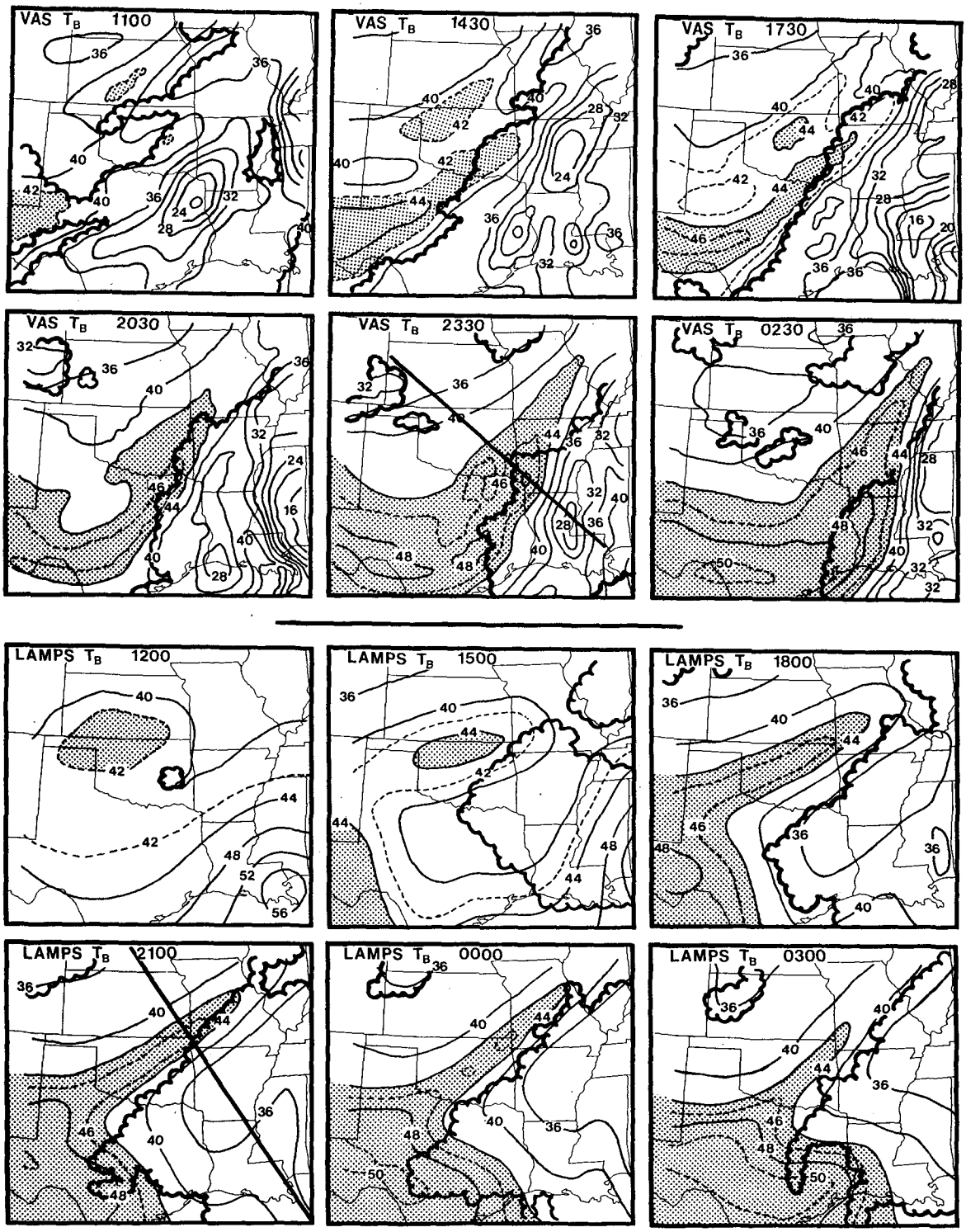

FIG. 3. Top: VAS T_B (kelvins −200, i.e., 36 denotes 236 K) corresponding to the water vapor images. Solid contours are at 4 K intervals while dashed lines indicate selected intermediate contours at 2 K intervals. Stippled areas within the 242 or 244 K contours approximately represent the dry bands. Areas within scallops denote VAS "split window" clouds. The straight solid line indicates the axis of a cross section in Fig. 10. Bottom: As in top except LAMPS T_B and areas within scallops denote model cloud water above 750 mb. The straight solid line indicates the axis of a cross section in Fig. 9.

advecting warm streak over western Texas at 1500 UTC, although it does not reproduce its observed narrow shape. At 1800 UTC, the simulated advective streak continues to intensify and propagate eastward over Texas. Its maximum T_B of 248 K compares favorably with the observed 246 K. Cold T_B's over eastern Texas, Arkansas, Louisiana and Mississippi correspond to cloudy regions. At 0000 UTC, the advective portion of the simulated imagery covers a substantial portion of Texas, and the cloudy area has continued to move eastward, ahead of the short-wave trough. Finally, at 0300 UTC, the leading edge of the advective feature has pushed into Louisiana, with maximum T_B's greater than 250 K over Texas. This aspect of the simulation shows excellent agreement with its observed counterpart.

LAMPS also does a credible job of modeling the development streak. At 1200 UTC (Fig. 3), the incipient model feature is denoted by a broadly shaped 242 K contour over the Kansas/Oklahoma border. By 1500 UTC, it has elongated, narrowed and intensified, coinciding with the northern lobe of the observed development feature. Unfortunately, however, the model does not simulate the second component over southeast Oklahoma. The lack of a double structure in the model's initial moisture field may explain this image deficiency. Indeed, Moore and Fuelberg (1988) and Stewart and Fuelberg (1986) found that even the special mesoscale rawinsonde network did not detect a double moisture signature. Thus, satellites can reveal structures not detected by conventional data, although the dual nature is not considered crucial in this particular case.

At 1800 UTC (Fig, 3), the simulated developing streak has a maximum T_B contour of 246 K, compared with an observed 244 K. The axis of the simulated band shifts slightly southeastward by 2100 UTC, similar to that observed; however, the former extends from southwest Oklahoma to central Illinois, while the latter stretches across southeast Oklahoma. The LAMPS development feature appears to weaken by 0000 UTC although its observed counterpart continues to intensify. This weakening is somewhat illusory, however, because unsmoothed T_B's (not shown) reveal a narrow axis, the width of a single grid point, along which values have not yet significantly decreased. Significant grid scale weakening of the model feature does not begin until after 0000 UTC. At the final time, 0300 UTC, the placement error has increased to approximately 200 km, with the simulated version extending from central Oklahoma to northeastern Missouri, and the observed version stretching from eastern Texas to southeastern Missouri.

In summary, LAMPS was successful in depicting many observed image structures. Therefore, model output will be used as a data source in calculations, as suggested by Keyser and Uccellini (1987). Frequent comparisons will be made with results from sonde data, with the goal being to infer causes for specific image features and their evolution.

b. Image, humidity, and kinematic relationships

To begin exploring atmospheric processes responsible for features observed in the water vapor imagery, LAMPS-derived 500 mb winds and absolute vorticity are examined (Fig. 4). Both the advecting (0300 UTC) and development (1500 UTC) image streaks occur primarily in the wakes of vorticity maxima, i.e., in areas of negative vorticity advection, where subsidence is expected. Trajectory analyses (section 5c) will examine

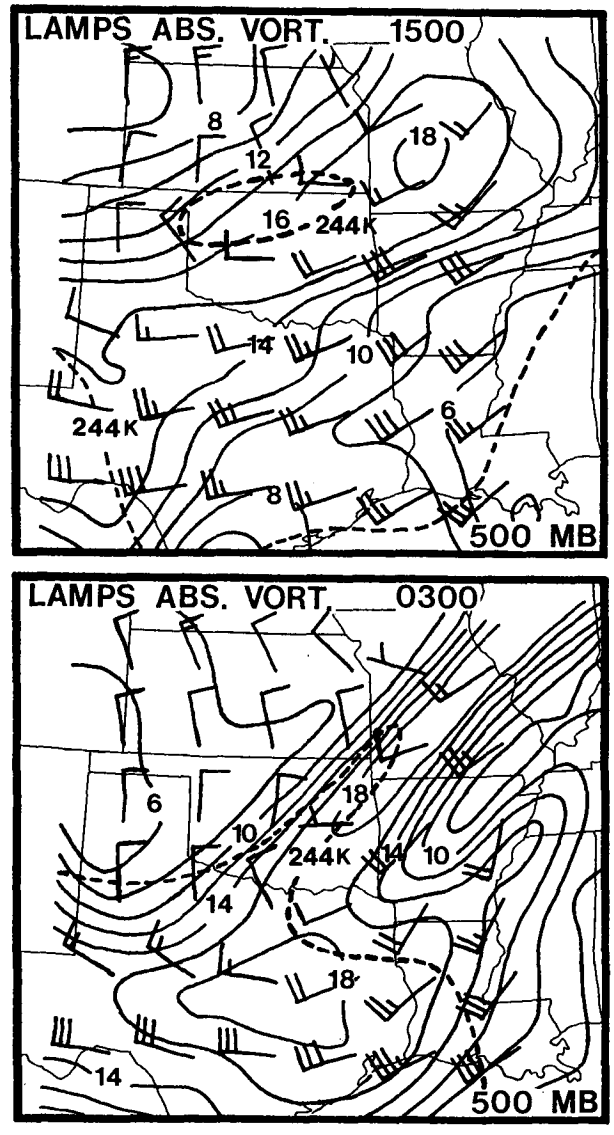

FIG. 4. LAMPS 500 mb winds (m s^{-1}) and absolute vorticity ($\times 10^{-5}$ s^{-1}) for UTC times indicated. Dashed line denotes 244 K T_B contour. Wind flags denote 50 m s^{-1}, long barbs 10 m s^{-1}, and short barbs 5 m s^{-1}.

processes by which leading edges of image streaks can move ahead of vorticity maxima and into regions of ascent.

Observed data corroborate relationships between the imagery and upper tropospheric flow patterns. Figure 5 displays 300 mb winds and T_B's. At 1430 UTC, the lobe of the development feature over western Oklahoma and southcentral Kansas is associated with the sharp cyclonic curvature of the shortwave trough. In their assessment of operational VAS products, Anthony and Wade (1983) reported that such troughs can be tracked by following dry image features. The component of the development band over southeastern Oklahoma is located in strong cyclonic speed shear northwest of the polar jet, while the advecting feature is associated with the jet maximum propagating into West Texas from the Desert Southwest. At 0230 UTC, the area encompassed by the 244 K contour is not symmetrical with the axis of maximum T_B. The axis appears to be associated with the strongest cyclonic wind shears.

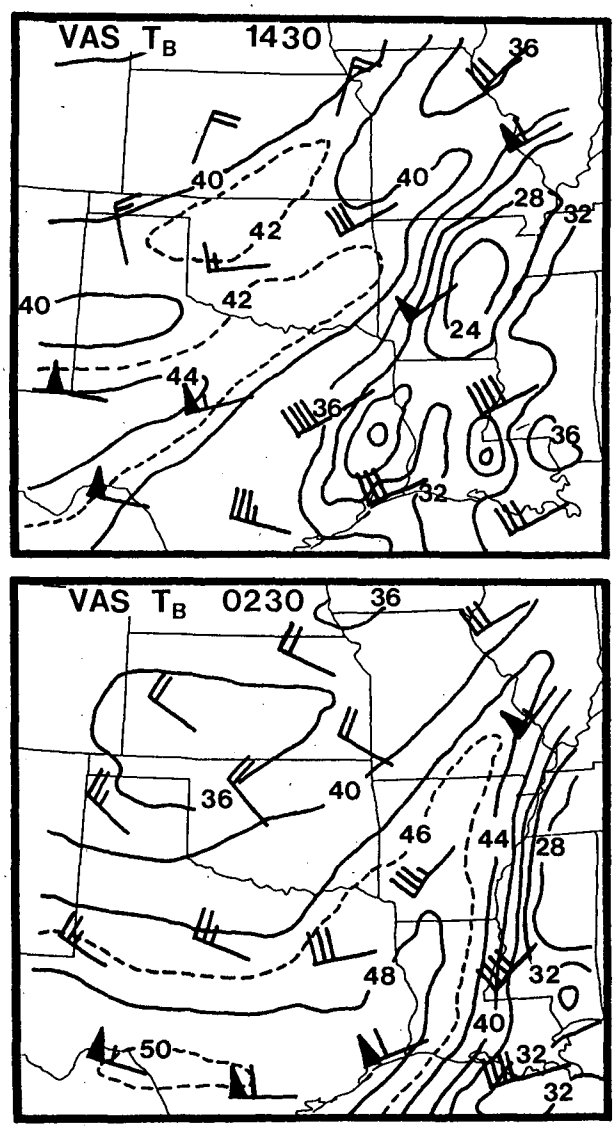

FIG. 5. 300 mb radiosonde-derived winds for 1445 and 0245 UTC superimposed on VAS T_Bs for 1430 and 0230 UTC. Winds are denoted as in Fig. 4.

Relationships between humidity and image features now will be explored. LAMPS-derived 500 mb vertical velocity and mixing ratio are examined at 1500, 2100, and 0300 UTC (Fig. 6), with RAOB-derived vertical motions at corresponding times included for comparison. One facet of using modeled data should be mentioned at the outset. Although T_B represents integrated temperature and humidity over the full depth of the model atmosphere, the model's coarse vertical resolution causes moisture values from any single level to affect a deep layer in the radiative simulation. Furthermore, sonde-derived humidity is absent and/or comparatively inaccurate in the upper levels, although it nonetheless serves as the LAMPS initial state. These factors result in a higher degree of similarity between LAMPS T_B (Fig. 3) and 500 mb water vapor patterns (Fig. 6) than is observed or expected between VAS imagery and sonde-derived patterns (not shown).

Mixing ratios (Fig. 6, center panels) depict the evolution of a broad area of dryness into a narrow zone, thereby suggesting deformation or confluence in airstreams near the trough axis. At 1500 UTC, values less than 0.4 g kg^{-1} over Oklahoma, Kansas, and the Texas Panhandle coincide with the incipient developing T_B feature. Furthermore, the model-derived subsidence maximum of -5 cm s^{-1} at this time (Fig. 6, top panels) coincides with areas of maximum T_B and minimum humidity. In general, the subsidence is west of the upper level trough (Fig. 1), while the cloudy southeastern portion of the domain is dominated by strong ascent. Sonde-derived vertical motions at 1445 UTC (Fig. 6, bottom panels) are similar qualitatively to the modeled version although the observed subsidence maximum is displaced slightly eastward, and it has the greater magnitude of -15 cm s^{-1}. Once again, however, the descent encompasses the developing image streak. Observed data confirm the strong ascent over Louisiana; however, weak ascent over the Texas Panhandle does not agree with model-derived weak subsidence.

The LAMPS analyses (Fig. 6) indicate that differential vertical motion at the early times helps form initial moisture gradients associated with the developing image feature and acts to deepen the upper level dry layer. In fact, calculations of moisture flux divergence (not shown) reveal that vertical transport in the 500 to 200 mb layer of this region dominates horizontal transport by an order of magnitude. This importance of vertical motion is illustrated by a cross section (Fig. 7) through the development feature at 1500 UTC (see

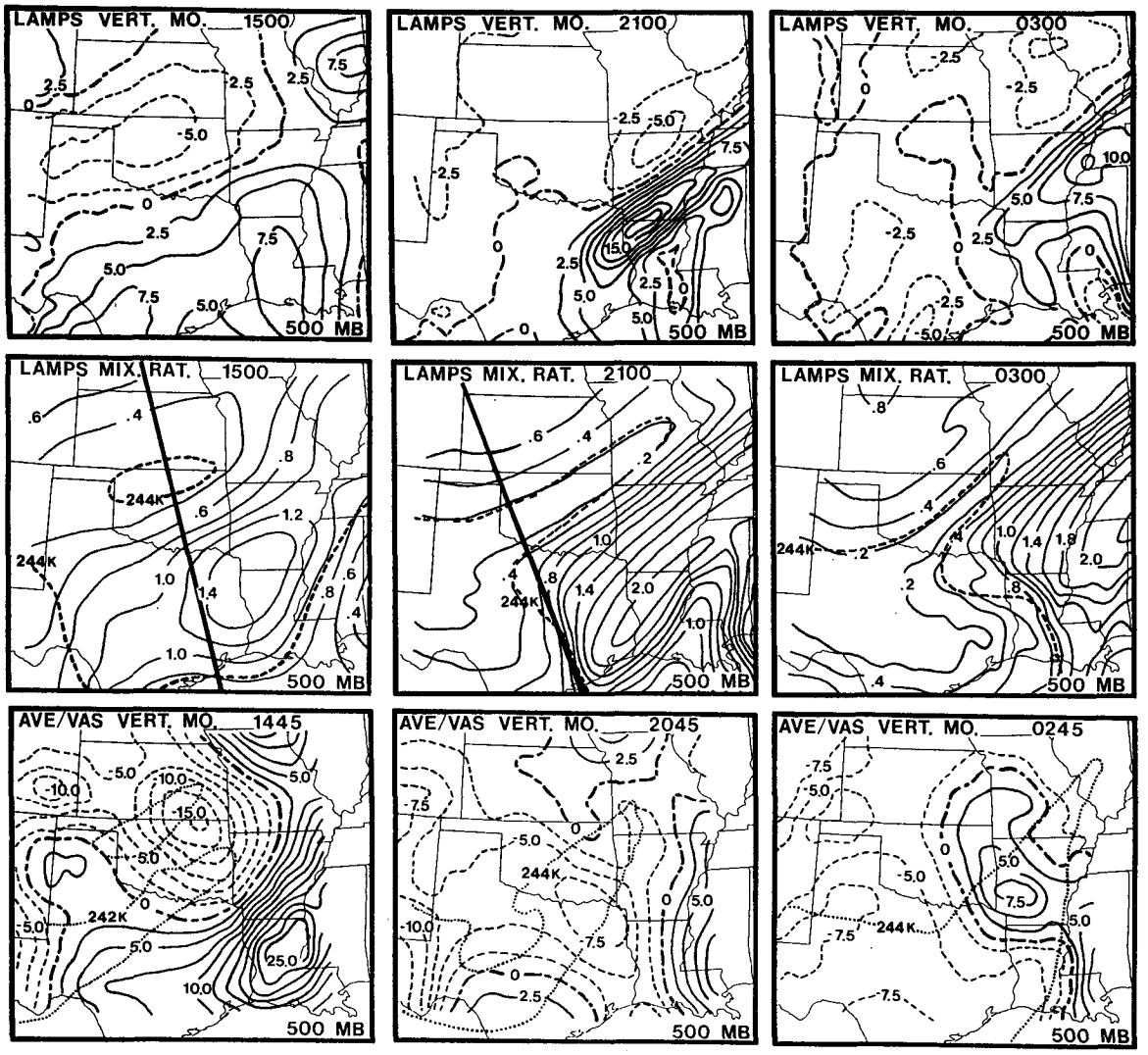

FIG. 6. Top: LAMPS 500 mb vertical velocity (cm s^{-1}), Middle: LAMPS 500 mb mixing ratio (g kg^{-1}), and Bottom: RAOB-derived (AVE/VAS) 500 mb vertical velocity (cm s^{-1}) for the times (UTC) indicated. For vertical velocity, dashed (solid) isolines indicate negative (positive) values while dash–dot denotes the zero line. Straight solid lines on mixing ratio plots indicate axes of cross sections in Figs. 7–8. Dashed lines on LAMPS mixing ratio plots indicate the 244 K T_B contour. Dotted lines on AVE/VAS plots indicate the 242 K or 244 K T_B contour.

axis in Fig. 6). It is clear that middle tropospheric subsidence over the northern (left) half of the diagram depresses moisture values in the region of warm T_B's constituting the developing image streak. The zero mixing ratio isoline marks the uppermost extent of model moisture. One should also note the relatively warm T_B's at the right (southern) edge of the figure. Since they correspond to greater upper tropospheric humidity than does the development feature, they apparently result from warmer ambient temperatures.

Moving forward in time, LAMPS-derived vertical motions at 2100 UTC (Fig. 6) indicate a slight northward protrusion of weak ascent into southwest Oklahoma near the junction of the development and advective features. Subsidence greater than -5 cm s^{-1} is found southeast of the development streak near the Arkansas/Missouri border while strong ascent from East Texas to southeastern Arkansas corresponds to clouds and precipitation. Meanwhile, the leading edge of the advecting image feature over southcentral Texas now extends eastward into the retreating region of ascent, suggesting that air which may have subsided previously now is being advected horizontally.

"Observed" vertical motions at 2045 UTC (Fig. 6) depict strongest ascent over southeast Louisiana and Mississippi, somewhat displaced from the modeled version. Subsidence dominates most other areas, with strongest values over western Texas. The earlier sub-

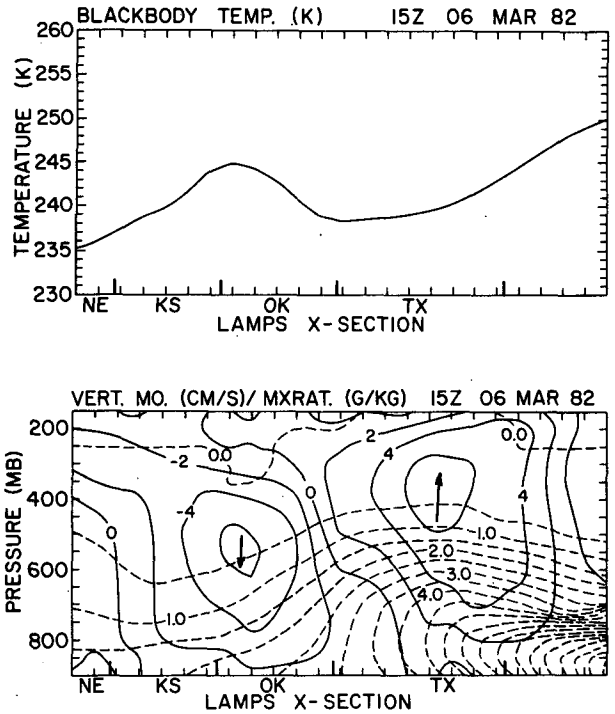

FIG. 7. Bottom: Cross section of LAMPS vertical velocity (solid, contours every 2.0 cm s^{-1}) and mixing ratio (dashed, contours every 0.5 g kg^{-1}). Locations for cross section are indicated in Fig. 6 at 1500 UTC. States are indicated at bottom of cross section separated by large tick marks. Top: LAMPS T_B (K) along the cross section.

sidence center over the Oklahoma/Kansas border has weakened and moved to northeastern Texas, coincident with the development image feature. LAMPS shows strong rising motion in this area, and this difference apparently is related to the error in trough placement. On the other hand, the observed cloud cover over East Texas (Fig. 3) and its position ahead of the short-wave trough do not support the eastward extension of "observed" subsidence.

When viewing water vapor imagery, it is tempting to assume that dark (warm) image areas denote centers of currently subsiding air; however, both modeled and observed results do not support such a simple interpretation at 2100 UTC. Figure 8 shows the displacement between centers of vertical motion and T_B in a nearly north–south cross section (axis in Fig. 6). For example, the T_B maximum of the development feature (center of the cross section) coincides with weak lower and middle tropospheric ascent. Above 500 mb, where vertical motions might strongly affect T_B's, warmest values do coincide with subsidence, but maximum descent is found far to the north (left) of the image streak. Warmest T_B is just south of the lowest level in the 0.5 g kg^{-1} mixing ratio isopleth, where the zero isopleth is nearest the surface. These differing locations between LAMPS-derived T_B and vertical velocity are consistent with previous model results. Durran and Weber (*1988*) found that differential vertical motions initially created moisture gradients, whereas subsequent vertical velocity patterns were very different from their model cirrus cloud boundaries.

Turning now to the last time (0300 UTC), one might attribute decay of the LAMPS development image feature to the weak ascent over southeastern Oklahoma (Fig. 6); however, T_B's near southern Missouri and northern Arkansas (Fig. 3) also decrease by an equal amount, and this is a region of -5 cm s^{-1} descent at 2100 UTC. Trajectory results (section 5c) will show that after formation of strong moisture gradients during early streak development, it is the origin of air parcels with respect to the gradients that controls T_B variations.

Regarding the model's advecting image feature at 0300 UTC (Fig. 6), its leading edge has moved into Louisiana, an area of ascent. This again suggests horizontal advection of previously subsided air, and once again, the image features cannot be equated with fields of instantaneous vertical velocity. This also is found in the observed vertical motions (Fig. 6), which again reveal descent over most of the domain although the maximum subsidence over Texas does correspond with the advecting streak. A somewhat puzzling item is the center of ascent over Arkansas that extends across the development band. Although similar ascent also occurs in the LAMPS patterns (Fig. 6), the sonde-derived center is considerably stronger (7.5 cm s^{-1} versus 2.5

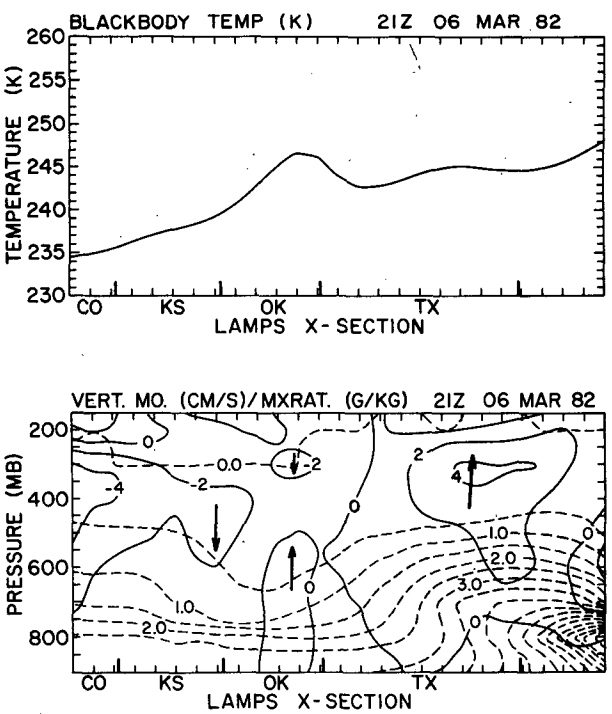

FIG. 8. As in Fig. 7 but for 2100 UTC.

cm s^{-1}). Based on IR satellite imagery, time continuity, and its location with respect to the short-wave trough, the magnitude of the observed ascent seems questionable, and could result from errors in the radiosonde winds, or aliasing of small scale features from the mesonetwork.

Evolution of the LAMPS dry regions (Fig. 6) is consistent with upper level frontogenesis and tropopause folding. Figure 9 (10) is a cross section of LAMPS-derived (sonde-derived) potential absolute vorticity (PAV) and T_B across the development image feature. Axis locations are shown in Fig. 3. Both versions indicate the downward sloping extrusion of stratospheric air (indicated by PAV greater than 10×10^{-6} K mb^{-1} s^{-1}) that is characteristic of tropopause folds (e.g., Reed 1955; Danielsen 1968). Moore and Fuelberg (1988) presented additional evidence for folding during this period. Ramond et al. (1981) found that warm T_B streaks associated with polar jet streams occurred near the "tropopause break," defined from a vertical cross section as "the furthest point reached poleward by the overhanging warm and moist subtropical air." Current results, however, indicate that maximum T_B is somewhat poleward of the break.

The current model scenario also agrees with earlier findings about the timing of upper level frontogenesis,

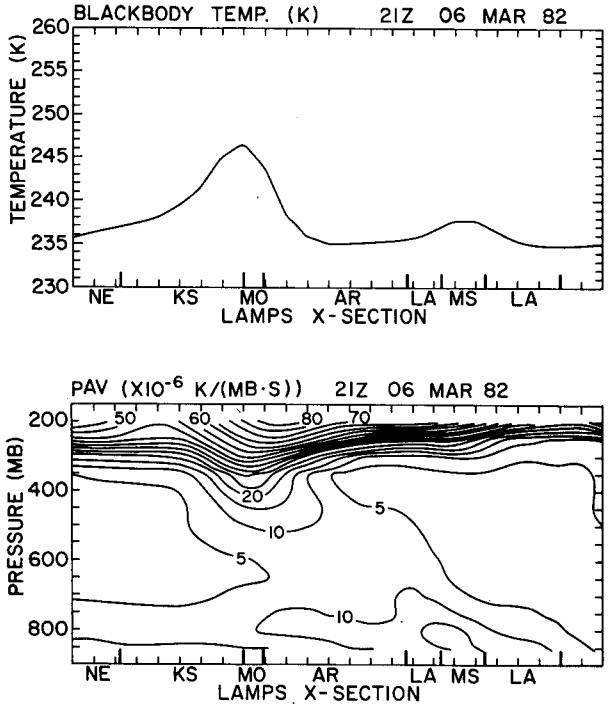

FIG. 9. Bottom: Cross section of LAMPS potential absolute vorticity (contours every 5×10^{-6} K mb^{-1} s^{-1}). Location of cross section indicated in Fig. 3 at 2100 UTC. States are indicated at bottom of cross section separated by large tick marks. Top: LAMPS T_B (K) along the cross section.

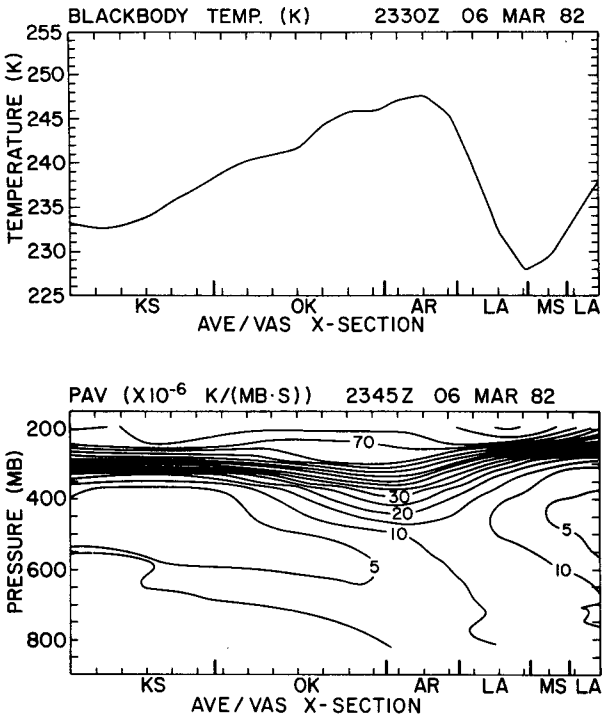

FIG. 10. Bottom: Cross section of RAOB-derived (AVE/VAS) potential absolute vorticity (contours every 5×10^{-6} K mb^{-1} s^{-1}) at 2345 UTC. Location for cross section indicated in Fig. 3 at 2330 UTC. States are indicated at bottom of cross section separated by large tick marks. Top: VAS T_B (K) along the cross section.

e.g., Bosart (1970), Keyser and Shapiro (1986) and others. Specifically, the 6–7 March period begins as the short wave passes through the major trough (Fig. 1), a configuration which Bosart found to be characterized by frontogenetical confluent horizontal processes and frontolytic thermally direct vertical circulations. In the current case, vertical motions produce the initial simulated dry image streak over Oklahoma (Fig. 3), which is then elongated by deformation.

c. *Trajectory analyses*

Parcel trajectories are a powerful tool for probing the image streaks. Basic flow characteristics are revealed by LAMPS-derived trajectories ending at 0300 UTC (Fig. 11a) and their sonde-derived counterparts ending at 0245 GMT (Fig. 11b). The trajectories, labeled 1–7 from left to right, end at 400 mb and are superimposed on the 244 K T_B contour that delineates the image bands. Values of water vapor and potential temperature associated with these air parcels are given in Table 1.

Model parcels ending west of the development streak (Fig. 11a) and behind the short-wave trough, move southward and descend, while parcels ending east of the streak ascend in the southwesterly jet flow. This

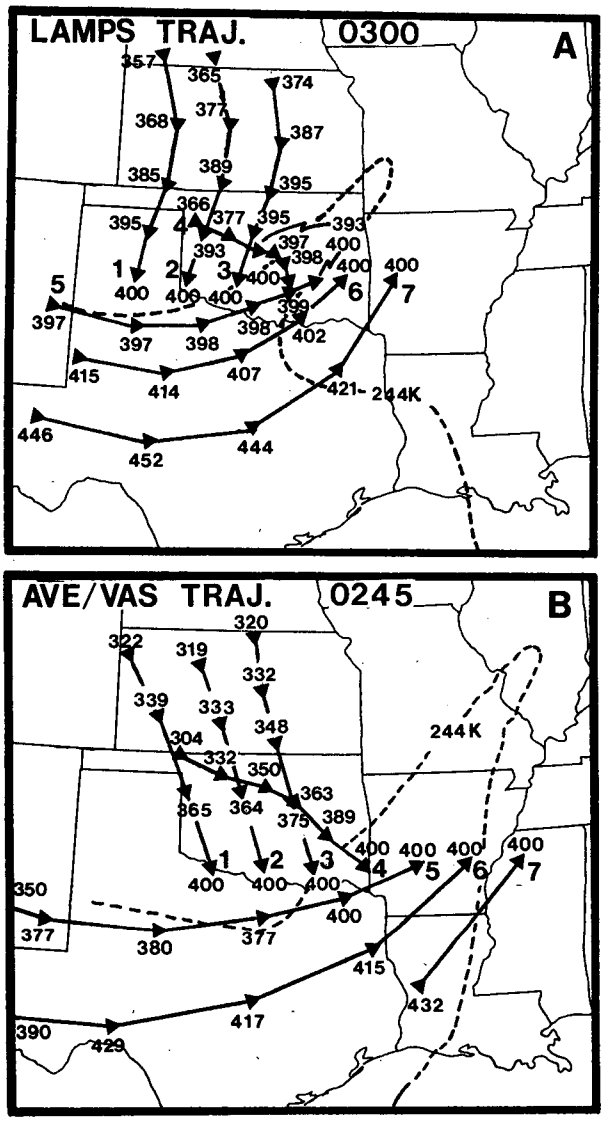

FIG. 11. (a) LAMPS trajectories ending at 400 mb on 0300 UTC 7 March computed over 3 hour increments. In both A and B, vertical positions of parcels are given in mb while dashed lines indicate the 244 K T_B contour. (b) AVE/VAS trajectories ending at 400 mb on 0245 UTC 7 March computed for time increments corresponding to the RAOB times.

confluence of airstreams appears responsible for the upper level frontogenesis described earlier (Fig. 9) and is similar to that discussed by Bosart (1970), Carlson (1980) and Durran and Weber (1988). Although broad scale aspects of the simulated flow are confirmed by the sonde-derived trajectories (Fig. 11b), AVE/VAS parcels ending west of the development streak do originate from a more northwesterly direction, and they undergo the greater vertical displacements expected from their larger vertical velocities (Fig. 6). For example, LAMPS parcels 1 and 2 subside 32 and 23 mb, respectively, between 1800 and 0300 UTC, while AVE/VAS parcels 1 and 2 sink 78 and 81 mb. In general, the LAMPS parcels conserve potential temperature and water vapor (Table 1) better than do the RAOB-derived versions, suggesting uncertainty in the kinematic vertical motions.

The two parcels labeled 4 are an interesting feature of the model- (Fig. 11a) and RAOB-derived (Fig. 11b) trajectories. In each case they come from the northwest, subside, and apparently move separately from airstreams ending on either side of them. Tracing their paths back through time, locations always coincide with the warm T_B area (Fig. 3), and they appear to accompany the short-wave trough. The LAMPS parcel subsides 27 mb between 1200 and 1800 UTC, but only 7 mb from 1800 to 0300 UTC. Similarly, the sonde-derived trajectory descends 46 mb in the first 7 h, 39 mb in the next 6 h, and only 11 mb during the final 3 h. Thus, as noted earlier, strong subsidence near the beginning of the period produces the dryness characterizing the warm image feature, but parcels comprising the streak do not undergo strong sinking throughout their histories. A comparison with Figs. 3, 10, and Moore and Fuelberg's (1988) Fig. 4 suggests that AVE/

TABLE 1. Top: LAMPS parcel variables corresponding to trajectories in Fig. 11a where p is pressure, w is mixing ratio, and θ is potential temperature. Bottom: RAOB-derived (AVE/VAS) parcel variables corresponding to trajectories in Fig. 11b.

Trajectory	Time (UTC)	p (mb)	w (g kg^{-1})	θ (K)
1	1500	357	0.14	308.3
	0300	400	0.15	307.8
2	1500	365	0.14	307.9
	0300	400	0.14	307.5
3	1500	374	0.11	307.2
	0300	400	0.10	307.1
4	1200	366	0.00	308.0
	0300	400	0.02	306.6
5	1200	397	0.11	307.4
	0300	400	0.08	306.7
6	1500	415	0.11	307.3
	0300	400	0.14	307.2
7	1500	446	0.15	310.0
	0300	400	0.34	309.4
1	1745	322	—	308.9
	0245	400	0.15	305.3
2	1745	319	—	309.9
	0245	400	0.13	305.4
3	1445	320	—	309.5
	0245	400	0.12	305.4
4	1100	304	—	315.9
	0245	400	0.13	305.7
5	1100	350	—	315.3
	0245	400	0.19	306.8
6	1445	390	0.14	316.7
	0245	400	0.28	309.0
7	2345	432	0.56	312.6
	0245	400	0.41	312.2

VAS parcel 4 (Fig. 11b) is within the upper portion of the tropopause fold. Parcel 5 also appears to be within the fold, but in contrast, moves rapidly in the westerly flow, originating at the leading edge of the advective streak in southwestern New Mexico.

We turn now to parcels specifically comprising the image streaks. Figure 12a contains six LAMPS-derived trajectories ending near the 465 mb sigma-height level at 2100 UTC. Thus, they describe the intensification period of the model development image feature. Figure 12b contains sonde-derived trajectories for similar locations with respect to the dry bands, while Table 2 gives vapor and potential temperature values associated with both versions of air parcels.

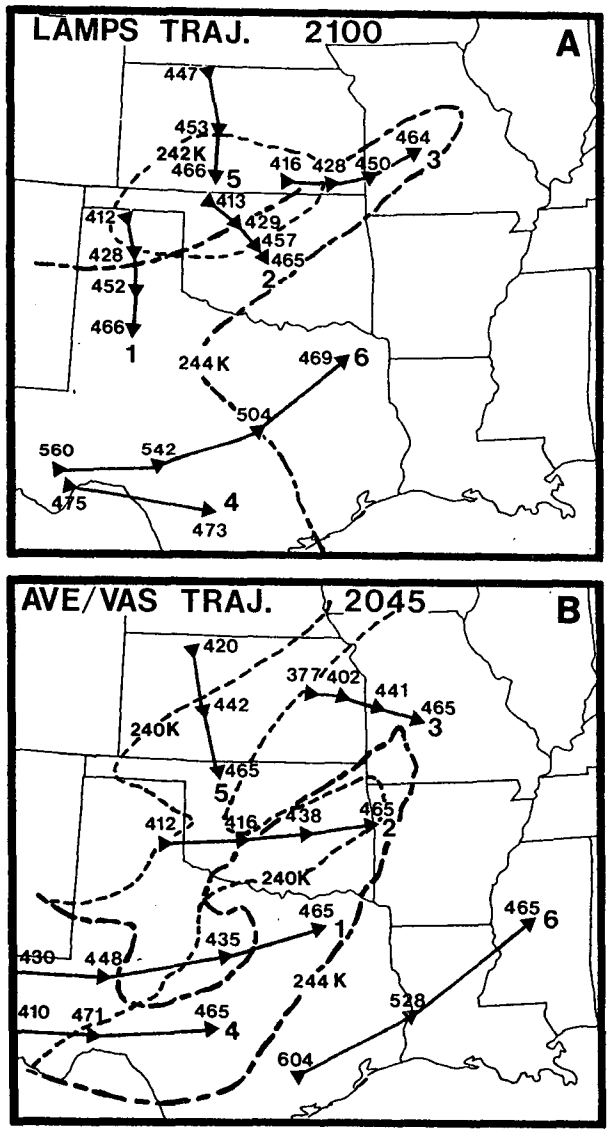

FIG. 12. (a) As in Fig. 11a but ending near 465 mb on 2100 UTC 6 March. Dashed lines indicate the 242 K T_B contour for 1200 UTC, and dash–dot indicates the 244 K T_B contour for 2100 UTC. (b) As in Fig. 11b but ending at 465 mb on 2045 UTC 6 March. Dashed lines indicate the 240 K T_B contour for 1100 UTC, and dash–dot indicates the 244 K T_B contour for 2030 UTC.

TABLE 2. Top: LAMPS parcel variables as in Table 1 corresponding to trajectories in Fig. 12a. Bottom: RAOB-derived (AVE/VAS) parcel variables corresponding to trajectories in Fig. 12b.

Trajectory	Time (UTC)	p (mb)	w (g kg^{-1})	θ (K)
1	1200	412	0.07	303.1
	2100	466	0.03	301.6
2	1200	413	0.07	303.5
	2100	465	0.04	302.4
3	1200	416	0.08	303.5
	2100	464	0.01	303.1
4	1800	475	0.26	311.7
	2100	473	0.21	311.9
5	1500	447	0.30	303.8
	2100	466	0.30	303.6
6	1200	560	1.43	307.3
	2100	469	0.85	308.4
1	1100	430	0.17	309.4
	2045	465	0.19	302.3
2	1100	412	0.11	301.4
	2045	465	0.19	301.7
3	1100	377	0.03	301.5
	2045	465	0.23	301.8
4	1445	419	0.18	312.7
	2045	465	0.21	304.9
5	1445	420	0.17	302.8
	2045	465	0.17	300.5
6	1445	604	2.76	306.3
	2045	465	1.22	315.4

LAMPS-derived trajectories 1, 2, and 3 end within the development streak (Fig. 12a), and can be traced back to the incipient warm T_B feature at 1200 UTC, thereby lending credibility to the calculations. In fact, these parcel locations are near the axis of maximum T_B at all times prior to 2100 UTC. Parcels 1 and 2 come from northerly or northwesterly directions, respectively, while parcel 3 comes from the southwest, thereby effecting the deformation of the dry pattern noted in Fig. 6. Young et al. (1987) observed a similar deformation that led to a "hammer head" shaped dry slot. In the current case, all three parcels originate at approximately 415 mb, subsiding nearly 50 mb during the 9 h period. One should note that the path from point 1 is nearly normal to the image streak, while that from point 3 is more parallel. This causes the base of the streak to move farther than its northern end, yielding the previously mentioned counterclockwise rotation. The final water vapor content of these parcels is small, ranging from 0.01 to 0.04 g kg^{-1} (Table 2) and they form the core of the dry area defining the development streak (Fig. 6).

Model parcel 5, ending northwest of the development band (Fig. 12a), can be traced back to 1500 UTC

before it leaves the domain. Between this time and 2100 UTC, however, it subsides only 19 mb, compared with 36 to 38 mb for parcels 1–3 that end within the dry image streak. More importantly, it contains 0.3 g kg^{-1} of water vapor, or nearly an order of magnitude more than parcels ending in the dry band. As noted in the humidity analyses (Fig. 6), this enhanced water vapor content defines the northwest edge of the image streak.

Southeast of the development feature (Fig. 12a), model parcel 6 ascends nearly 90 mb between 1200 and 2100 UTC in the southwesterly flow ahead of the short wave. It is located within the cloudy region and ends with the comparatively large mixing ratio of 0.85 g kg^{-1}. Finally, trajectory 4, located within the advective streak, can be traced back only to 1800 UTC due to the strong jet flow. Although the parcel is associated with T_B's greater than 248 K at 2100 UTC, it actually ascends 2 mb during the 3 h period, corroborating the findings of Rodgers et al. (1976) that some dry image areas result from the horizontal transport of previously subsided air.

Sonde-derived trajectories ending at 2045 UTC (Fig. 12b) confirm many aspects of the simulated versions (Fig. 12a). For example, trajectories 2–3 that end near or within the observed dry feature also originate within them at 1100 UTC. On the other hand, these paths are more westerly than those from LAMPS, and the deformation pattern is not seen as clearly. Sonde-derived paths well behind the trough (parcel 5) again are northerly. Parcels 1 and 4 are embedded within the jet flow accompanying the advective streak (Fig. 12b), remaining within the warm T_B boundaries (Fig. 3), and both ascending and descending during their passage through the computational domain. Parcel 6, meanwhile, reflects the vigorous southwesterly ascent into the stormy region over the Gulf states, rising 139 mb in 6 h, and ending with a mixing ratio of 1.22 g kg^{-1} (Table 2).

Dissipation of the model development streak now will be examined. Figure 13 presents trajectories ending near 465 and 500 mb at 0300 UTC while Table 3 presents associated variables. LAMPS parcels 1 and 2 (Fig. 13a) continue to follow the movement of the image feature, i.e., their locations at each time are at or near the core of maximum T_B. During the 15 h period prior to 0300 UTC, they have subsided 61 and 55 mb, respectively, ending with very dry mixing ratios of 0.03 and 0.04 g kg^{-1}, respectively. Although parcel 3 sinks nearly as much (52 mb), it originated northeast of the incipient dry region, in an area of greater upper tropospheric humidity. Thus, its mixing ratio of 0.14 g kg^{-1} is considerably greater than values for parcels 1–2. This influx of water vapor into southwestern Missouri produces a progressively smaller dry region (Fig. 6) and the weakening of the developing image feature.

Most of the subsidence experienced by LAMPS parcels 1 and 2 occurs early in their histories (Fig. 13a),

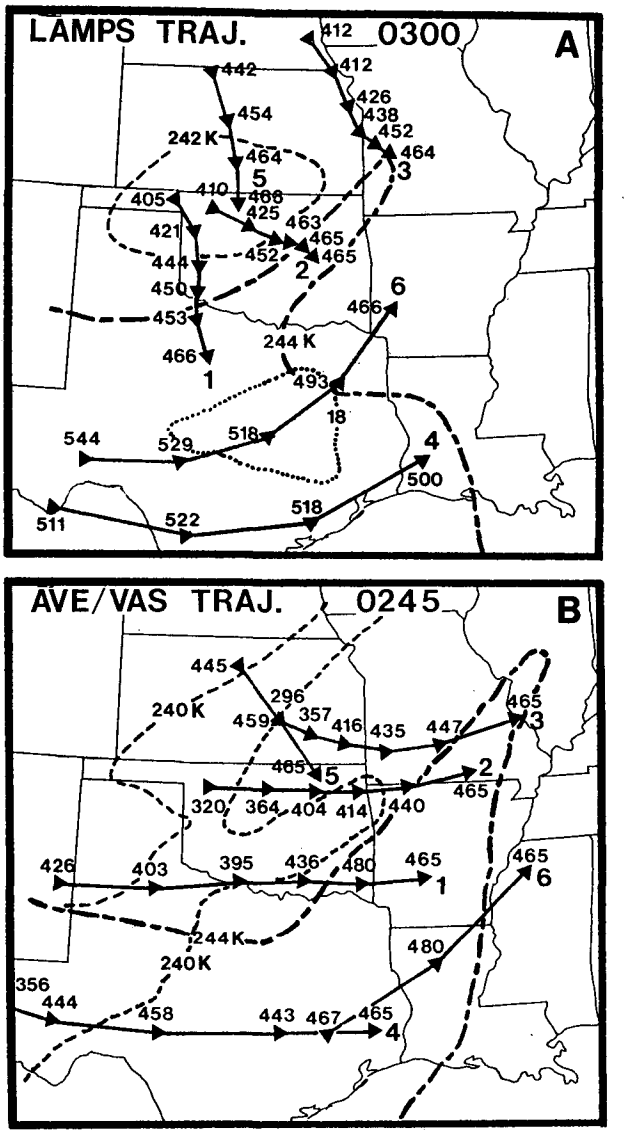

FIG. 13. (a) As in Fig. 11a but ending near 465 mb (or 500 mb for parcel 4) on 0300 UTC 7 March. Dashed lines indicate the 242 K T_B contour for 1200 UTC, and dash-dot indicates the 244 K T_B contour for 0300 UTC. Dotted line indicates the 18×10^{-5} s^{-1} absolute vorticity contour for 0300 UTC. (b) As in Fig. 11b but for 0245 UTC 7 March. Dashed lines indicate the 240 K T_B contour for 1100 UTC and dash-dot indicates the 244 K T_B contour for 0230 UTC.

similar to that described at 2100 UTC (Fig. 12a). Northwest of the development feature, parcel 5 sinks as much as parcels 1–2 during the final 6 h period, indicating a decrease in the differential subsidence which caused initial dry (warm) band development. Meanwhile, parcel 6 undergoes rapid ascent, with a mixing ratio an order of magnitude greater than those within the dry areas.

In contrast to the simulated development feature (Fig. 3), the observed version continues to strengthen

TABLE 3. Top: LAMPS parcel variables as in Table 1 corresponding to trajectories in Fig. 13a. Bottom: RAOB-derived (AVE/VAS) parcel variables corresponding to trajectories in Fig. 13b.

Trajectory	Time (UTC)	p (mb)	w (g kg^{-1})	θ (K)
1	1200	405	0.05	303.9
	0300	466	0.03	302.2
2	1200	410	0.07	304.0
	0300	465	0.04	302.4
3	1200	414	0.18	304.2
	0300	464	0.14	304.3
4	1800	511	0.65	310.0
	0300	500	0.50	310.7
5	1800	442	0.39	304.2
	0300	466	0.39	304.2
6	1500	544	1.01	305.4
	0300	466	0.68	306.1
1	1100	426	0.14	301.3
	0245	465	0.19	302.1
2	1100	320	—	313.2
	0245	465	0.15	302.0
3	1100	296	—	316.6
	0245	465	0.20	303.5
4	1445	356	0.18	319.2
	0245	465	0.20	307.4
5	2045	445	0.20	303.1
	0245	465	0.19	301.7
6	2045	467	0.49	309.1
	0245	465	0.73	308.3

through 0245 UTC. RAOB-derived trajectories ending at 465 mb 0245 UTC (Fig. 13b) track parcels 2–3 almost due westward, back to the dry air comprising the warm bands at 1100 UTC. They originate in the northwestern component of the observed development feature, subside 145 mb and 169 mb, respectively, between 1100 and 0245 UTC, with strongest descent occurring prior to 1745 UTC. Once again it appears that strong subsidence early in the period is the major contributor to the development feature. Unfortunately, it is impossible to compare these results with those of parcel 5, located northwest of the development streak, because it moved out of the domain before 2045 UTC. AVE/VAS parcel 6, southeast of the development feature, shows little change in pressure level.

The evolution of the simulated advecting image feature also should be described near the ending time of 0300 UTC. LAMPS parcel 4 (Fig. 13a) ends at 500 mb near the maximum of absolute vorticity (18×10^{-5} s^{-1}). Comparison with prior vorticity charts (not shown) reveals that the parcel descends 11 mb west of the maximum vorticity between 1800 and 2100 UTC. It passes nearly horizontally south of the vorticity center, and then ascends 18 mb from 0000 to 0300 UTC, moving eastward ahead of the vorticity maximum toward the leading edge of the image streak. An apparently similar process resulted in cyclically descending and ascending modeled trajectories in a dry airstream during the Presidents' Day Storm (Whitaker et al. 1988). Although previous investigators have noted ascent in the northern tips of dry slots (e.g., Danielsen 1980; Young et al. 1987; Carr and Millard 1985; Leese 1962), current results indicate that it also occurs along their eastern edges.

Referring now to sonde-derived trajectories near the advecting feature (Fig. 13b, Table 3), AVE/VAS parcel 4 remains within that streak during the entire period, while parcel 1 ends in Arkansas near the merging region of the two image features. Between 1100 and 0245 UTC, parcel 1 experiences both ascent and descent, arriving after a net subsidence of only 40 mb and a potential temperature increase from 301.3 K to 302.1 K. During the same period, parcel 4 undergoes an unsteady descent from 356 to 465 mb. The large decrease in potential temperature from 319.2 K to 307.4 K again casts doubt upon the reliability of the kinematic vertical motion estimates. Neither parcel reflects the more uniform subsidence characterizing those within the recently formed development streak.

As the final point, it is useful to consolidate previous material and explain evolutionary differences between the simulated and observed development image features (Fig. 13). One major difference is the smaller eastward movement of the modeled dry band. This is due mostly to weaker LAMPS-derived upper tropospheric winds, depicted as closer 3 h successive parcel positions. Related to this location error is the model's failure to strengthen adequately the image feature as it does advance. The explanation can be seen by comparing the two versions of trajectories 1–3. The sonde-derived versions (Fig. 13b) originate 15 h earlier in the incipient developing feature. They then move eastward, eventually meeting parcels from the southwest that had comprised the advecting image area. A merger of the two image bands results. With the LAMPS simulation (Fig. 13a), however, the northeastern edge of the development feature consists of parcels (e.g., parcel 3) that originate outside of the incipient dry area at 1200 UTC. Thus, at 0300 UTC they are transporting relatively humid air into this tip of the image streak, causing it to dissipate. In addition, LAMPS parcels 1–2 travel in a southeasterly, not easterly, direction. Thus, they merge with parcels from the advecting feature over northern Texas and southeastern Oklahoma, instead of farther eastward. If model winds and resulting trajectories had been only slightly different, T_Bs in the simulated development band might have continued to increase.

6. Conclusions

LAMPS mesoscale model simulation and 3-hour radiosonde data have been used to investigate pronounced warm (dry) bands in 6.7 μm water vapor imagery on 6–7 March 1982. Model soundings were input

to a radiative transfer algorithm to generate fields of synthetic 6.7 μm equivalent black body temperatures (T_B) which were compared with those from the VAS sensor aboard GOES. The purpose was to reveal processes resulting in the formation and evolution of the dry image features.

LAMPS captured major aspects of the observed imagery, including development and advective image features and a cold cloud area. On the other hand, the model did not resolve some finer scale details such as the observed double structure of the development streak, perhaps because it was not detected in the initial moisture analysis (Moore and Fuelberg 1988; Stewart and Fuelberg 1986). Although LAMPS reproduced several evolutionary aspects of the imagery, including intensification and eastward propagation of the advective component over Texas and rotation of the development feature, it did not duplicate observed continuous strengthening of the development portion. Furthermore, the simulated version was displaced approximately 200 km from its observed counterpart by the end of the period. Greatest differences between modeled and observed T_B images occurred in regions of cloud cover. In locations where LAMPS reproduced clouds reasonably accurately, these differences could be ameliorated by incorporating a cloud algorithm into the radiative transfer procedure. The T_B contrasts outside of cloudy regions were comparatively small.

LAMPS analyses showed that water vapor content generally was the dominant factor determining T_B's in cloud free regions. Ambient temperature variability had a noticeable impact at times, however, causing relatively warm T_B's to occur in areas of enhanced humidity. This temperature dependence of 6.7 μm imagery frequently is overlooked during their interpretation.

LAMPS output was a valuable tool for explaining image configurations. Model trajectories showed good qualitative agreement with those calculated from 3-hour sonde data. Differing wind fields, discrepancies in vertical motion, differences in initial moisture patterns, and lack of model vertical resolution helped explain contrasting results between simulated and observed imagery. Nonetheless, the fact that the model captured many aspects of the observed streaks, combined with the self-consistency between model T_B's and dynamics, allow findings to be synthesized.

The development image feature formed along an upper level short wave as it moved through a major trough. The axis of maximum T_B was located within the region of maximum vorticity. Thus, the image feature formed within negative vorticity advection and the resulting subsidence that is expected from quasi-geostrophic theory (e.g., Holton 1979). Initial moisture gradients were enhanced by strong differential subsidence during the first 6 h of the study period, thereby intensifying the image feature. In addition, horizontal deformation accompanying the short wave caused the dry area to elongate along the trough line. This was simulated as narrowing of a single, initially oval shaped warm (dry) area into a long, narrow streak. In the observed case, deformation caused the narrowing and merger of two distinct image components into a single entity. Cross sections of potential absolute vorticity showed a downward extrusion of stratospheric air accompanying the dry development band, similar to those seen previously during upper level frontogenesis and tropopause folding. In fact, this evolution appears consistent with Bosart's (1970) finding about upper level frontogenesis during the latter stages of a disturbance's movement through a major trough. After strong subsidence had formed the dry streak, horizontal transport played a major role in producing the upper tropospheric variability. Thus, T_B patterns could not be equated to a "snapshot" of the vertical velocity fields because some dry air that had originally subsided also moved horizontally or even rose.

The advective image feature also was associated with an upper level vorticity maximum, this time from cyclonic speed shear accompanying a polar jet streak around the major trough. Because air comprising the warm image band was traveling faster than the vorticity field itself, parcels sank in the rear of the vorticity maximum, moved through it, and then rose in its leading edge. Even though parcels were rising, however, they retained their dry characteristics, still yielding the warm T_B feature.

Both model and observed trajectories indicated northerly or northwesterly subsiding flow behind the development feature and north of the advective portion. Conversely, air streams east and southeast of the image features generally were ascending, while parcels ending within the development feature moved with it. These latter parcels had subsided during much of their paths. They moved separately from other air streams and appeared to lie within the zone of stratospheric air defining the tropopause fold. The slowly moving air within the development streak advanced at a large angle with respect to its axis, resulting in southeastward propagation. On the other hand, air within the advecting feature was moving parallel to its orientation. For the observed streak, this resulted in a rapid eastward and northeastward movement, and eventual merging with the development component.

Quasi-geostrophic theory and the knowledge that image streaks can delineate middle level waves provide a simple framework for better understanding previous research. For example, Young et al. (1987) and Carr and Millard (1985) found that ascent at the northern tip of a dry image region led to "dry slot convection." Similarly, Petersen et al. (1984) observed a tendency for thunderstorms to develop along the edges of middle level warm (dry) bands when they overlie areas of moisture. They speculated that a probable decrease in

subsidence along these edges would provide less resistance to convection. Current model trajectories, however, indicate that air near the leading edge of an image streak may, in fact, be rising since it is ahead of the vorticity maximum associated with the upper level short wave. Thus, a dry band can not only denote convective instability if it moves over low level moisture, but it also can be associated with the upper level disturbance that may "trigger" the instability.

This case study has attempted to clarify the upper tropospheric kinematics associated with a commonly observed signature in water vapor imagery. Such imagery often is available at 1–3 h intervals, providing mesoscale information that is unobtainable from conventional data. Current associations between shortwave troughs and warm T_B features describe a strongly dynamic period; however, further research is needed to determine whether these results are applicable to other cases, e.g., those without strong dynamics and baroclinicity. By showing that image features are manifestations of specific atmospheric processes, studies such as this can benefit both forecasters and researchers.

Acknowledgments. The authors thank Drs. Franklin Robertson and Michael Kalb of NASA's Marshall Space Flight Center for providing the LAMPS dataset and for numerous helpful discussions. The kind help of the following people is also appreciated: Drs. Michael Weinreb and Michael Hill of NOAA/NESDIS, who provided the radiative transfer code, and Ms. Cynthia Wheatley-Lovoy, Ms. Caroline Poore, and Mr. Dewey Rudd of FSU, who assisted with manuscript preparation. Thanks also are due to Dr. James McGuirk for his helpful review of this work. The research was sponsored by NASA through Grant NAG8-033 under the auspices of the Remote Sensing Branch of the Marshall Space Flight Center. The assistance of our grant monitor Dr. Gary Jedlovec is much appreciated.

REFERENCES

Anthony, R. W., and G. S. Wade, 1983: VAS operational assessment findings for spring 1982/83. *Preprints, 13th Conf. Severe Local Storms.* Tulsa, Amer. Meteor. Soc., J23–J28.

Barnes, S. L., 1973: Mesoscale objective map analysis using weighted time-series observations. National Severe Storms Laboratory, Norman, OK, 73069, 60 pp. [NTIS COM-73-10781.]

Bosart, L. F., 1970: Mid-tropospheric frontogenesis. *Quart. J. Roy. Meteor. Soc.*, **96,** 442–471.

Carlson, T. N., 1980: Airflow through midlatitude cyclones and the comma-cloud pattern. *Mon. Wea. Rev.*, **108,** 1498–1509.

Carr, F. H., and J. P. Millard, 1985: A composite study of comma clouds and their association with severe weather over the Great Plains. *Mon. Wea. Rev.*, **113,** 370–387.

Chesters, D., L. W. Uccellini and A. Mostek, 1982: VISSR Atmospheric Sounder (VAS) simulation experiment for a severe storm environment. *Mon. Wea. Rev.*, **110,** 198–216.

Danielsen, E. F., 1968: Stratospheric–tropospheric exchange based on radioactivity, ozone and potential vorticity. *J. Atmos. Sci.*, **25,** 502–518.

——, 1980: Stratospheric source for unexpectedly large values of ozone measured over the Pacific Ocean during Gametag, August, 1977. *J. Geophys. Res.*, **85,** 401–412.

Durran, D. R., and D. B. Weber, 1988: An investigation of the poleward edges of cirrus clouds associated with midlatitude jet streams. *Mon. Wea. Rev.*, **116,** 702–714.

Fischer, H., N. Eigenwillig and H. Muller, 1981: Information content of METEOSAT and Nimbus/THIR water vapor channel data: Altitude association of observed phenomena. *J. Appl. Meteor.*, **20,** 1344–1352.

Fuelberg, H. E., and P. J. Meyer, 1986: An analysis of mesoscale VAS retrievals using statistical structure functions. *J. Climate Appl. Meteor.*, **25,** 60–75.

Heckley, W. A., and B. J. Hoskins, 1982: Baroclinic waves and frontogenesis in a nonuniform potential vorticity semi-geostrophic model. *J. Atmos. Sci.*, **39,** 1999–2015.

Holton, J. R., 1979: *An Introduction to Dynamic Meteorology.* 2nd ed., Academic Press, 391 pp.

Jedlovec, G. J., 1985: An evaluation and comparison of vertical profile data from the VISSR Atmospheric Sounder (VAS). *J. Atmos. Oceanic Technol.* **2,** 559–581.

Kalb, M. W., 1987: The role of convective parameterization in the simulation of a Gulf Coast precipitation system. *Mon. Wea. Rev.*, **115,** 214–234.

Keyser, D., and M. A. Shapiro, 1986: A review of the structure and dynamics of upper-level frontal zones. *Mon. Wea. Rev.*, **114,** 452–499.

——, and L. W. Uccellini, 1987: Regional models: emerging research tools for synoptic meteorologists. *Bull. Amer. Meteor. Soc.*, **68,** 306–320.

Leese, J. A., 1962: The role of advection in the formation of vortex cloud patterns. *Tellus*, **14,** 409–421.

Liou, K., 1980: *An Introduction to Atmospheric Radiation.* Academic Press, 392 pp.

Moore, S. R., and H. E. Fuelberg, 1988: Relations between water vapor imagery, vertical motion, and tropopause folds. *Preprints, 3rd Conf. Satellite Meteorology and Oceanography,* Anaheim, Amer. Meteor. Soc., 203–208.

O'Brien, J. J., 1969: Alternative solutions to the classical vertical velocity problem. *J. Appl. Meteor.*, **9,** 197–203.

Perkey, D. J., 1976: A description and preliminary results from a fine-mesh model for forecasting quantitative precipitation. *Mon. Wea. Rev.*, **104,** 1513–1526.

Petersen, R. A., L. W. Uccellini, A. Mostek and D. Keyser, 1984: Delineating mid- and low-level water vapor patterns in preconvective environments using VAS moisture channels. *Mon. Wea. Rev.*, **112,** 2178–2198.

——, and J. H. Homan, 1989: Short-range forecasting and nowcasting using a simple, isentropic prediction model. *Wea. Forecasting,* **4,** 5–23.

Petterssen, S., 1956: *Weather Analysis and Forecasting, Vol. 1,* McGraw-Hill, 428 pp.

Poc, M. M., M. Roulleau, N. A. Scott and A. Chedin, 1980: Quantitative studies of Meteosat water-vapor channel data. *J. Appl. Meteor.*, **19,** 868–876.

Ramond, D., H. Corbin, M. Desbois, G. Szejwach and P. Waldteufel, 1981: The dynamics of polar jet streams as depicted by the METEOSAT WV channel radiance field. *Mon. Wea. Rev.*, **109,** 2164–2176.

Reed, R. J., 1955: A study of a characteristic type of upper-level frontogenesis. *J. Meteor.*, **12,** 226–237.

——, and M. Albright, 1986: A case study of explosive cyclogenesis in the eastern Pacific. *Mon. Wea. Rev.*, **114,** 2297–2319.

Rodgers, D. M., M. J. Magnano and J. H. Arns, 1985: Mesoscale convective complexes over the United States during 1983. *Mon. Wea. Rev.*, **113,** 888–901.

Rodgers, E. B., V. V. Salomonson and H. L. Kyle, 1976: Upper tropospheric dynamics as reflected in Nimbus 4 THIR 6.7 μm data. *J. Geophys. Res.*, **81,** 5749–5758.

Shuman, F. G., 1957: Numerical methods in weather prediction. II: smoothing and filtering. *Mon. Wea. Rev.*, **85**, 357–361.

Smith, W. L., 1983: The retrieval of atmospheric profiles from VAS geostationary radiance observations. *J. Atmos. Sci.*, **40**, 2025–2035.

Stewart, M. R., and H. E. Fuelberg, 1986: Relationships between 6.7 micrometer imagery and radiosonde derived parameters. *Preprints, 2nd Conf. Satellite Meteorology/Remote Sensing and Applications,* Williamsburg, Amer. Meteor. Soc., 67–72.

Uccellini, L. W., K. F. Brill and C. H. Wash, 1985: The President's Day cyclone of 18–19 February 1979: Influence of upstream trough amplification and associated tropopause folding on rapid cyclogenesis. *Mon. Wea. Rev.*, **113**, 962–987.

Velden, C. S., 1987: Satellite observations of Hurricane Elena (1985) using the VAS 6.7 μm "water-vapor" channel. *Bull. Amer. Meteor. Soc.*, **68**, 210–215.

Weinreb, M. P., and A. C. Neuendorffer, 1973: Method to apply homogeneous-path transmittance models to inhomogeneous atmospheres. *J. Atmos. Sci.*, **30**, 662–666.

——, and M. L. Hill, 1980: Calculation of atmospheric radiances and brightness temperatures in infrared window channels of satellite radiometers. NOAA Tech. Rep. NESS 80, U.S. Dept. of Commerce, 40 pp. [Available from the authors at NOAA/NESDIS, Washington, D.C. 20233.]

Weldon, R. and S. Holmes, 1984: Characteristics of water vapor imagery. Unpublished manuscript, 32 pp. [available from NOAA/NESDIS, Washington, D.C. 20233.]

Whitaker, J. S., L. W. Uccellini and K. F. Brill, 1988: A model-based diagnostic study of the rapid development phase of the President's Day cyclone. *Mon. Wea. Rev.*, **116**, 2337–2365.

Young, M. V., G. A. Monk, and K. A. Browning, 1987: Interpretation of satellite imagery of a rapidly deepening cyclone. *Quart. J. Roy. Meteor. Soc.*, **113**, 1089–1115.